

Decoding and quantitative detection of antibiotics by a luminescent mixed-lanthanide-organic framework

Yuping Wang¹, Jing Xia², Yanxin Gao (✉)¹

¹ Department of Environmental Science and Engineering, Fuzhou University, Minhou 350108, China

² State Environmental Protection Key Laboratory of Environmental Risk Assessment and Control on Chemical Process, School of Resources and Environmental Engineering, East China University of Science and Technology, Shanghai 200237, China

HIGHLIGHTS

- A series of mixed-LOFs and portable LOF-fibers were synthesized.
- LOF-S3 was selected as a luminescent sensor for antibiotics.
- Mixed-LOF was capable of decoding antibiotics by emission intensity ratios.
- Linear relationship between antibiotic concentration and I545nm/I618nm was observed.

ARTICLE INFO

Article history:

Received 19 December 2021

Revised 14 April 2022

Accepted 6 May 2022

Available online 17 June 2022

Keywords:

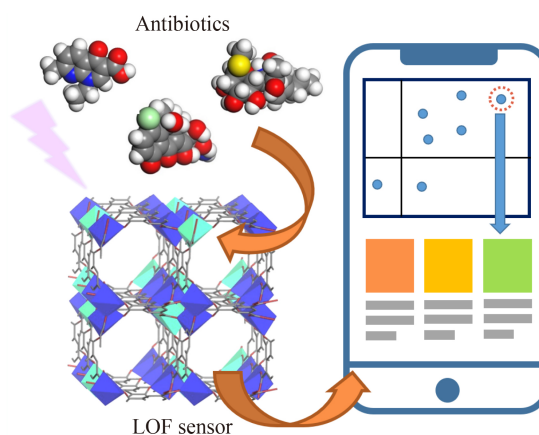
Antibiotics

Sensor

Luminescence

Lanthanide-organic frameworks

GRAPHIC ABSTRACT



ABSTRACT

Due to the potential risk of antibiotics to the environment, the development of inexpensive, simple, and reliable antibiotic detection methods is significant but also faces challenges. In this work, several lanthanide-organic frameworks (LOFs), constructed from lanthanide ions (Eu^{3+} and/or Tb^{3+}) and 1,3,5-benzene-tricarboxylic acid (BTC), were synthesized by solvothermal method. LOF-S3 with comparable emission peaks of ${}^5\text{D}_4 \rightarrow {}^7\text{F}_5$ (Tb^{3+} , 545 nm) and ${}^5\text{D}_0 \rightarrow {}^7\text{F}_2$ (Eu^{3+} , 618 nm) was selected as a luminescent sensor. In this system, the highly efficient energy transferred from the organic linker to lanthanide ions and from Tb^{3+} to Eu^{3+} occurs. LOF-S3 sensor was capable of decoding antibiotics by distinguishable emission intensity ratios. Therefore, a two-dimensional decoded map of antibiotics was established. The linear relationship between antibiotic concentration and emission intensity ratio indicated the quantitative determination of antibiotics was feasible. As a typical analyte, the response mechanism of nalidixic acid (NA) was investigated in detail. The competition of NA and BTC for UV light absorption, as well as the binding propensity of NA and Tb, affected the organic linkers-to-lanthanide ions and Tb-to-Eu energy transfer, resulting in the change of fluorescence intensity ratio. The self-calibrating mixed-LOF sensor overcame the uncontrollable errors of the traditional absolute emission intensity method and generated stable luminescent signals in multiple cycles. Furthermore, the integration of LOF-S3 with polymer fibers enabled the formation of a LOF-polymer fibrous composite with fluorescence detection capability, which is a promising portable sensor for practical applications.

© Higher Education Press 2022

✉ Corresponding author

E-mail: gaoyx20@fzu.edu.cn

Special Issue—Emerging Contaminants: Science and Policy (Responsible Editors: Bin Wang, Qian Sui, Haoran Wei, Damià Barceló & Gang Yu)

1 Introduction

Used extensively in the treatment of bacterial infections, antibiotics have been regarded as an emerging type of organic contaminants in the aquatic environment (Cheng

et al., 2020; Kovalakova et al., 2020; Xu et al., 2021). Since antibiotics residues can be released into the natural water through wastewater treatments, various antibiotics have been detected in surface water, groundwater, and drinking water (Hu et al., 2021; Wang et al., 2021). Probing and monitoring these emerging contaminants are significant but challenging. To date, the detection of antibiotics has mainly relied on instrumental analysis such as mass spectrometry, liquid chromatography with UV detection, and capillary electrophoresis (Hernández et al., 2003; Chiesa et al., 2018; Roth et al., 2021). However, all these methods are expensive, time-consuming, and need trained personnel. Therefore, the development of inexpensive, simple, and reliable methods to detect antibiotics effectively has attracted great concern from researchers.

With the advantages of low-energy consumption, easy operation, and high efficiency, optical sensing has been regarded as a promising technology in the detection of antibiotics. The main challenge in the development of optical sensing is the synthesis and selection of photo-responsive materials. Due to the 4f electrons in lanthanide (Ln) ions, luminescent lanthanide compounds possess unique photo-electronic properties, including sharp and stable emission signals, long luminescence lifetimes, and large absorption/emission energy gaps, which provide a great opportunity for optical sensing (Eliseeva and Bünzli, 2010). Yet the relatively weak light absorption capacity of Ln ions and the Laporte-forbidden 4f-4f transition lead to low quantum yields and insufficient luminescent brightness. Thus, lanthanide compounds cannot be used for sensing directly (Moore et al., 2009).

As a new class of self-assembled porous materials, metal-organic frameworks (MOFs) have been applied in diverse fields, including molecular sensing (Dolgoplova et al., 2018; Kökçam-Demir et al., 2020; Wu et al., 2020). MOFs can be systematically modified by adjusting metal ions/organic linkers or implanting different functionalities. Therefore, coordination of organic linkers and lanthanide ions/clusters can generate lanthanide-organic frameworks (LOFs). Owing to the synergistic effect of MOFs and Ln ions, LOFs show unique optical properties (Xia et al., 2020). In addition, the suitable organic linkers in LOFs can serve as chromophoric sensitizers to greatly enhance the light absorption ability and increase the luminous brightness via the “antenna effect” (Moore et al., 2009). It has been reported that the energy transfer pathway and efficiency from the “antenna” to the Ln nodes could be affected by the host-guest interactions. Therefore, a lot of LOFs can sensitively respond to the contained guest molecules as a luminescent probe (Hou et al., 2019; Yang et al., 2019). However, as most of the currently studied luminescent LOFs are based on changes in the absolute emission intensity of a single Ln ion, their sensitivity is not sufficiently accurate, and they lack the ability to recognize different molecules. To expand the

applications of LOFs, similar Ln ions are incorporated into one framework to form mixed-lanthanide-organic frameworks. Recent elaborations have demonstrated that after tuning the proportion of Ln ions in mixed-LOFs, the distinguishability of luminescent signals will be remarkably improved, resulting in different luminescent colors in detection (Zhan et al., 2014; Yu et al., 2021). Zeng and colleagues prepared a mixed-lanthanide metal-organic framework Tb/Eu(TATB) for the visual detection of F⁻ in drinking water (Zeng et al., 2020). Karmakar and co-workers reported the synthesis of $\{[\text{Tb}_{1-x}\text{Eu}_x(\text{L})(\text{DMF})(\text{H}_2\text{O})] \cdot 1.5\text{H}_2\text{O}\}_n$ and its application in Cu²⁺ sensing (Karmakar et al., 2021). In addition, with the property of induced-fit-type structural conversion, some LOFs can ensnare different molecules by modulating their channel shape and/or pore size to adapt to the host-guest interactions. The different host-guest interactions can be further transformed into unique luminous signals.

Despite the advantages, reports on the applications of mixed-lanthanide-organic frameworks are still limited. In our previous work, we found that mixed-LOFs can be applied to fluorescence ratiometric detection of pharmaceuticals (Gao et al., 2018). However, this material is not durable enough in aqueous solution. Considering that the structure based on 1,3,5-benzenetricarboxylic acid (BTC) and lanthanide ions is flexible, a more stable sensor can be obtained by adjusting the synthesis conditions and the coordination state. Therefore, in this work, we modulated the synthesis process and prepared a series of durable mixed-LOFs. 13 widely used antibiotics were chosen as the guest molecules, containing β -lactams, tetracyclines, amphenicols, lincomycin, sulfonamides, and quinolones. The mixed lanthanide-organic framework sensor LOF-S3 presented a remarkable property that recognized different antibiotics by emission intensity ratios (Tb ⁵D₄ → ⁷F₅ transition to Eu ⁵D₀ → ⁷F₂ transition). A two-dimensional (2D) decoded map for antibiotics was established according to the intensity ratio changes. The sensor emitted differentiable luminescence for each antibiotic in the visible light region arising from dynamic structural transformations and various host-guest interactions, which modulated the energy transfer path, efficiency and allocation. The quantitative analysis of antibiotics and its mechanism were also studied. In addition, to prepare a portable sensor for real-world applications, we explored the integration of LOFs with polymer fibers to enable the formation of LOF-polymer fibrous composites. MOF-fibers are attractive in air/water purification, personal protective equipment, biomedical devices and sensing applications due to improved transport of molecules through the material and easier access to the active sites of MOFs (Peterson et al., 2021). We investigated the stability and durability of LOF-polymer fibers and used it to detect nalidixic acid. To our knowledge, this is the first report on the preparation of mixed-LOF fibers for antibiotic detection using fluorescence ratios. Our work proposed a promising portable self-calibrating sensor for beneficial applications.

2 Materials and methods

2.1 Materials

BTC, $\text{Tb}(\text{NO}_3)_3 \cdot 6\text{H}_2\text{O}$, and $\text{Eu}(\text{NO}_3)_3 \cdot 6\text{H}_2\text{O}$ were all purchased from Sigma-Aldrich (USA). Solvent dimethylformamide (DMF) and ethanol were offered by Peking Reagent (China). 13 antibiotics (chloramphenicol, chlorotetracycline, lincomycin, nalidixic acid, penicillin, sulfamethoxazole, tetracycline, trimethoprim, sulfadiazine, sulfamerazine, sulfaclozine, sulfameter, and sulfachinoxalin) were all obtained from Dr. Ehrenstorfer GmbH (Germany).

2.2 Preparation of LOFs

The Tb(or Eu)-BTC was synthesized by adding H_3BTC (0.40 mmol), $\text{Tb}(\text{NO}_3)_3 \cdot 6\text{H}_2\text{O}$ (or $\text{Eu}(\text{NO}_3)_3 \cdot 6\text{H}_2\text{O}$) (0.28 mmol), ethanol (8 mL), and deionized water (8 mL) to a vessel. After vigorous stirring, white crystals of Ln-BTC were formed and collected by centrifugation, washed thoroughly with DMF and methanol, and dried at 100 °C for 12 h. For the synthesis of mixed-LOFs, EuTb-BTC, certain amounts of corresponding lanthanide nitrates ($\text{Tb}(\text{NO}_3)_3 \cdot 6\text{H}_2\text{O}$ and $\text{Eu}(\text{NO}_3)_3 \cdot 6\text{H}_2\text{O}$) were added to the reaction system. The as-synthesized samples were named LOF-S1, LOF-S2, LOF-S3, LOF-S4, LOF-S5, LOF-S6, LOF-S7, and LOF-S8. The molar ratios of Eu to Tb in these samples were 1:50, 1:25, 1:12, 1:5, 1:3, 1:2, 1:1, and 4:1, respectively.

2.3 Characterization of LOFs

The X-Ray Diffraction (XRD) patterns of LOFs were collected on a D/MAX-RBX-ray diffractometer (Rigaku, Japan) with a Cu-K α radiation source. Scanning Electron Microscope (SEM) (Zeiss, Germany) was used to obtain images of the samples and analyze morphology. It was operated at 15 kV with a magnification of 500–10000. The FT-IR spectra of LOFs were recorded on a Thermo Nicolet Nexus 870 FT-IR spectrometer system (Thermo Fisher, USA) to confirm the functionality. Thermogravimetric analysis (TGA) was carried out under a N_2 atmosphere on a TGA/DSC instrument (Mettler Toledo, Switzerland) at a heating rate of 10 °C/min. Luminescence spectra of the solid samples were recorded on a fluorescence spectrometer (Hitachi F7000, Japan) at room temperature. The photomultiplier tube voltage was 500 V with a scan speed of 2400 nm/min. The corresponding optical photographs were taken by a DM6000B fluorescence microscope (Leica, Germany) equipped with a D-UV filter.

2.4 Luminescence sensing

An activated sample of mixed Ln-BTC (1 mg) was added

to 50 mL of 100 $\mu\text{mol/L}$ prepared solution at room temperature and reacted for 60 min. The mixture was centrifuged, followed by separation, washing and drying of the solid sample. Then the powder was analyzed with a fluorescence spectrometer and a fluorescence microscope. To estimate the relationship between the concentration and the emission intensity ratio, 1–150 $\mu\text{mol/L}$ solutions of antibiotics were used. For recycling experiments, the solid samples were washed thoroughly with methanol and dried by a rotating evaporator to remove the adsorbed molecules. Nalidixic acid was used as the representative analyte to investigate the sensing mechanism and test the performance of LOF-fibers.

2.5 Preparation of mixed-LOF fibrous composite

The integration of mixed-LOF and polymers was based on the MOF-first method, where the synthesis and deposition of LOF occur prior to fiber formation. 0.26 mmol $\text{Tb}(\text{NO}_3)_3 \cdot 6\text{H}_2\text{O}$, 0.02 mmol $\text{Eu}(\text{NO}_3)_3 \cdot 6\text{H}_2\text{O}$, 0.40 mmol H_3BTC , 8 mL deionized water, and 8 mL ethanol were added in vessel. After vigorous stirring, the products were separated by centrifugation, washed with methanol, and dried in a vacuum oven. To form the mixed-LOF fibrous composite, the electrospinning technique was used. A certain amount of Ln-BTC was added into 5 mL DMF. The dose of Ln-BTC can be adjusted to optimize the LOF-loading on the fibers. The suspension was sonicated for 10 min to disperse LOF crystals. 0.2 g polyvinyl pyrrolidone (PVP) and 0.2 g polyacrylonitrile (PAN) were added to 5 mL DMF. The mixture was heated in an oil bath at 60 °C and stirred vigorously for 3 h. After electrospinning, the fibrous composite was immersed in ethanol aqueous solution at 50 °C for 12 h to remove PVP. Finally, the fibers were washed and dried in a vacuum oven for 12 h.

3 Results and discussion

Needle-like crystals of Ln-BTC were prepared by the reaction of H_3BTC and lanthanide nitrate. The characterization of Ln-BTC was based on FT-IR, XRD, SEM, and TGA. Fig. 1(a) shows the XRD patterns of crystallized Tb-, Eu-, mixed EuTb-BTC and the simulated spectrum according to the single-crystal X-ray diffraction data of Ln-BTC from other work (Shu et al., 2022). The peaks of the as-synthesized sample are matched with the peaks from the simulated spectrum without additional peaks, demonstrating that mixed-LOF is a pure phase crystal and Eu- and Tb-BTC are isomorphous. In FT-IR spectra (Fig. S1), the broad peak centered at 3435 cm^{-1} corresponds to the stretching vibrations of the O-H bonds. The sharp peaks at 1380 and 1537 cm^{-1} are attributed to the symmetric (ns(C-O)) and asymmetric (nas(C-O)) vibrations of the carboxyl groups, respectively (Horcajada

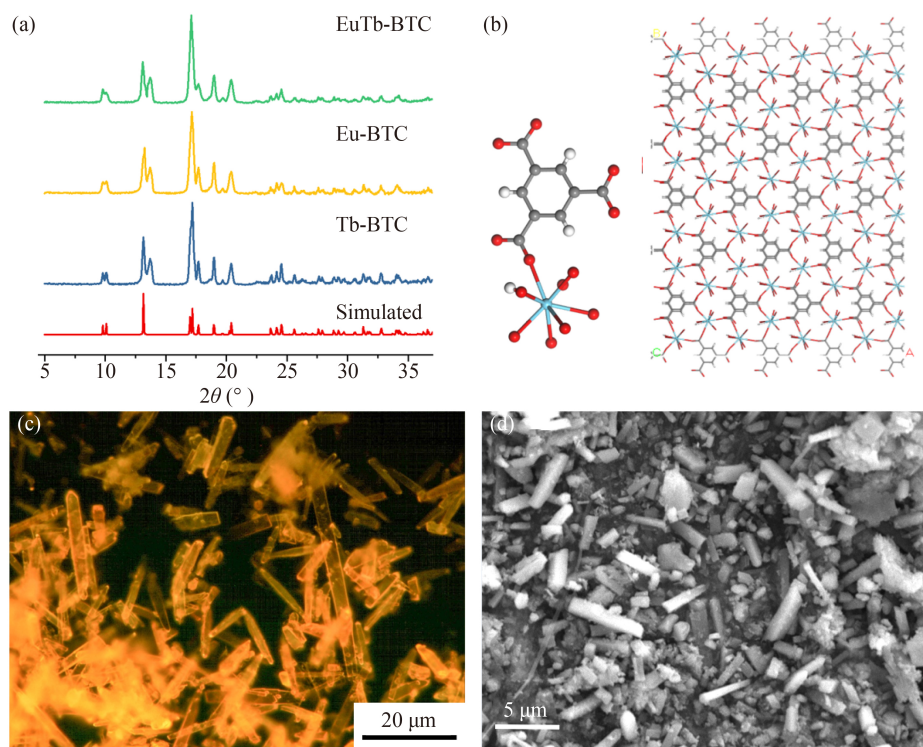


Fig. 1 (a) XRD spectra of Ln-BTC; (b) the coordination state of the Ln ion and the structure of Ln-BTC (Tb and/or Eu, blue; O, red; C, gray); (c) fluorescence microscope photograph of mixed-Ln-BTC; (d) SEM image of mixed-Ln-BTC.

et al., 2008), suggesting the existence of the dicarboxylate in the sample. The schematic internal structure shown in Fig. 1(b) reveals that they form a rather complicated overall topology due to the tritopic nature of the organic secondary building units. The Ln-O-C units are constructed from coordinated Ln(III) centers. As shown in the model, terminal water ligand and carboxyl groups are bound to Ln clusters. The crystals were also observed by fluorescence microscope and SEM. As exhibited in Figs. 1(c) and 1(d), the bulky crystals of mixed Ln-BTC emit orange light with irradiation and a long rod-like morphology with a diameter of about 1 μm and a length of 10–50 μm. Table S1 shows the surface elemental composition of a mixed-LOF, LOF-S3. The atomic percentage of Eu is about 7.4%, consistent with the dosage of Eu nitrate during the synthetic process. The TGA curve in Fig. S2 reveals the excellent thermal stability of Ln-BTC, of which the decomposition temperature is above 500 °C.

According to the previous reports (Zhan et al., 2014; Zeng et al., 2020), the most obvious characteristic peaks of Tb³⁺ and Eu³⁺ in the luminescence spectrum are located at 545 nm and 618 nm. Therefore, the emission intensity under different excitation wavelengths was monitored at 545 nm (Tb) and 618 nm (Eu) to determine the optimal excitation wavelength. As shown in Fig. S3, for Tb-BTC and Eu-BTC, the effective excitation wavelengths are at the range of 270–290 nm, which is mainly related to the maximum absorbance of the organic

linker BTC. Thus, 286 nm was selected as the excitation wavelength for Ln-BTCs. As for lanthanide salts, the optimal excitation wavelength is much longer, where Tb(NO₃)₃·6H₂O is 355 nm and Eu(NO₃)₃·6H₂O is 395 nm. Fig. 2(a) shows the emission spectra of the solid Tb(NO₃)₃·6H₂O sample and Tb-BTC powder measured at their optimal excitation wavelengths. Both Tb(NO₃)₃·6H₂O and Tb-BTC exhibit the characteristic emission bands of Tb³⁺ at 488, 545, 587, and 622 nm in the luminescence spectra, attributed to the ⁵D₄ → ⁷F₆, ⁵D₄ → ⁷F₅, ⁵D₄ → ⁷F₄, and ⁵D₄ → ⁷F₃ transitions, respectively. As for Eu(NO₃)₃·6H₂O and Eu-BTC (Fig. 2(b)), both of them exhibit the characteristic peaks of Eu³⁺ in the luminescence spectra: ⁵D₀ → ⁷F₀ (592 nm), ⁵D₀ → ⁷F₂ (618 nm), ⁵D₀ → ⁷F₃ (654 nm), and ⁵D₀ → ⁷F₄ (703 nm). However, Ln-BTCs exhibit much stronger and sharper characteristic luminescence emission bands than pristine lanthanide salts. The results demonstrated that the emission intensities of the LOFs were dramatically enhanced due to the binding of organic ligands. The calculated quantum yields of 69.9% (Tb-BTC) and 30.3% (Eu-BTC) excited at 286 nm are much higher than that of 14.7% (Tb(NO₃)₃·6H₂O) excited at 355 nm and 14.8% (Eu(NO₃)₃·6H₂O) excited at 395 nm, respectively (Supplementary material 1. Quantum yield measurements). These results confirm that the energy is efficiently transferred from BTC to Tb³⁺/Eu³⁺. The excitation energy of Ln ions is closely matched with the emission energy of BTC to achieve the “antenna effect” (Brites

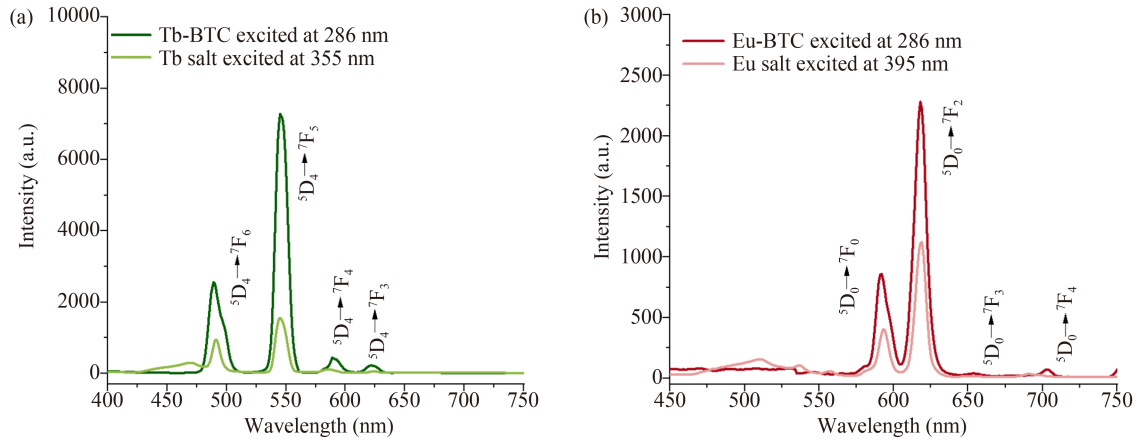


Fig. 2 Emission spectra for (a) $\text{Tb}(\text{NO}_3)_3 \cdot 6\text{H}_2\text{O}$ and Tb-BTC, (b) $\text{Eu}(\text{NO}_3)_3 \cdot 6\text{H}_2\text{O}$ and Eu-BTC.

et al., 2010). However, the emission intensity of Eu-BTC was much lower than that of Tb-BTC excited at 286 nm, which indicated that the energy transfer from BTC to Eu^{3+} was less efficient than that from BTC to Tb^{3+} (Brites et al., 2010). The photoluminescence decay curves of Eu-BTC and Tb-BTC ($\lambda_{\text{ex}} = 286 \text{ nm}$) were collected at 618 and 545 nm, respectively (Fig. S4). The photoluminescence decay curves are well fitted by the double exponential decay model, and the average lifetime is calculated by the Eq. (1):

$$\tau_{\text{av}} = \frac{A_1\tau_1^2 + A_2\tau_2^2}{A_1\tau_1 + A_2\tau_2}, \quad (1)$$

where τ_1 and τ_2 are the fluorescence lifetimes for the fast and slow decay processes, respectively. A_1 and A_2 are the pre-exponential factors for the fitted curve. The τ_{av} of Eu-BTC is 0.637 ms, and τ_{av} of Tb-BTC is 1.209 ms (Table S4). The energy transfer behavior between lanthanide ions in mixed-LOF system can be analyzed by comparing the decay curves for Tb-BTC (545 nm), Eu-BTC (618 nm) and EuTb-BTC (545 and 618 nm). The average decay times of the Eu^{3+} and Tb^{3+} ions are determined to be 0.756 and 0.664 ms in mixed EuTb-BTC, respectively (Fig. S7 and Table S4). It can clearly be seen that in the mixed-LOF sample the average lifetime of Eu^{3+} becomes longer, while that of Tb^{3+} becomes shorter compared to

the single lanthanide sample. The above results indicate that the energy transfer from Tb^{3+} to Eu^{3+} occurs (Zhang et al., 2016b). The efficiency of energy transfer (η_T) from Tb^{3+} to Eu^{3+} ions can be estimated by the equation: $\eta_T = 1 - \tau_{(\text{Tb in EuTb-BTC})} / \tau_{(\text{Tb in Tb-BTC})}$. Thus, the η_T is determined to be 45.1%. Since the average lifetime of Eu^{3+} is extended from 0.637 ms (Eu-BTC) to 0.664 ms (EuTb-BTC), Eu^{3+} is the energy transfer acceptor in the mixed-LOF. In this system, light absorption, energy transformation, and emissivity were well balanced, effective linker-metal/metal-metal energy transfer and protection of Ln ions from non-radiative decay leading to intense luminescence (Chatterton et al., 2005).

Through adjusting the ratios of Eu^{3+} to Tb^{3+} during the synthesis process, the luminescent colors of these mixed-LOFs were systematically modulated. As shown in Fig. 3(a), excited at 286 nm, Ln-BTCs (Tb-BTC, LOF-S1-8, and Eu-BTC) display tunable luminescence emission spectra via weakening or enhancing the corresponding emission intensities of Tb^{3+} and Eu^{3+} . In the spectrum of LOF-S3, the characteristic peaks of two lanthanide ions are comparable. Taking the integrated emission intensity ratio $I_{545 \text{ nm}} / I_{618 \text{ nm}}$ ($\text{Tb}^{3+} \ ^5\text{D}_4 \rightarrow \ ^7\text{F}_5$ transition to $\text{Eu}^{3+} \ ^5\text{D}_0 \rightarrow \ ^7\text{F}_2$ transition) as the standard, its value is close to 1. Therefore, LOF-S3 is the most suitable material for sensing. Corresponding to the

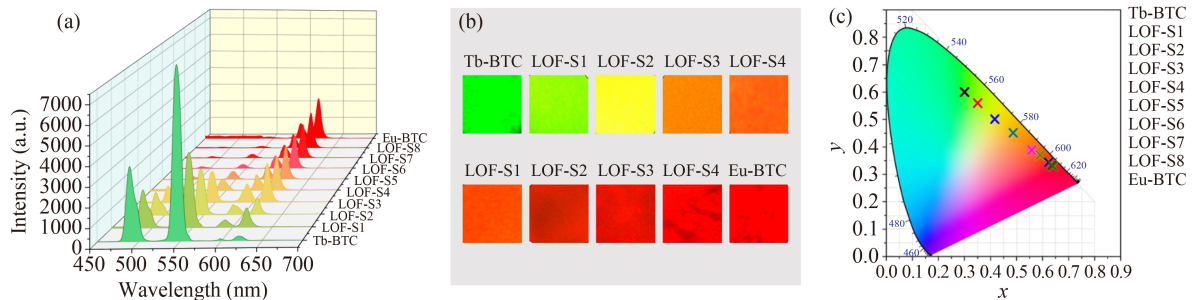


Fig. 3 (a) Luminescent spectra of Ln-BTCs ($\lambda_{\text{ex}} = 286 \text{ nm}$) in the solid-state at room temperature; (b) the optical photographs for LOF samples under fluorescence microscope; (c) CIE chromaticity coordinates.

change of emission intensity ratio, the color of LOFs observed under the fluorescence microscope changed from green to red (Fig. 3(b)). As can be seen from the 1931 Commission Internationale de L'Eclairage (CIE) chromaticity diagram (Fig. 3(c)), the emission colors match well with the calculated chromaticity coordinates.

In the luminescence spectra of $\text{Eu}_x\text{Tb}_{1-x}\text{-BTC}$, the emission energy of lanthanide ions was transferred from BTC by excitation. Therefore, we expected that the efficiency of energy transfer would respond to the adsorbed molecules due to the host-guest interactions. The guest-dependent luminescence of Ln-BTC is the basis for decoding different antibiotics. Since the emission intensities of lanthanide ions in LOF-S3 ($\lambda_{\text{ex}} = 286 \text{ nm}$) were comparable, we used LOF-S3 as a sensor for probing different antibiotics and investigated its luminescent property. To detect antibiotics, obtained LOF-S3 was immersed in 100 $\mu\text{mol/L}$ different antibiotic solutions (chloramphenicol, chlortetracycline, lincomycin, nalidixic acid, penicillin, sulfamethoxazole, tetracycline, and trimethoprim) for 30 min at room temperature. Fig. S5 indicates that antibiotics themselves do not show luminescence when excited at 286 nm. Thus, the luminescent signal comes from the mixed-LOF sensor. As shown in Fig. 4(a), the solid samples of LOF-S3 exhibit different emission spectra after antibiotic sensing. For example, nalidixic acid shows a quenching effect for the emission of Eu^{3+} but a dramatic enhancing effect for Tb^{3+} , while tetracycline mainly quenches the emission of Tb^{3+} . As the emission spectra of mixed-LOF are highly dependent on the guest molecules, it is an excellent candidate of luminescent sensor by establishing fingerprint correlation between antibiotics and emission intensity ratios. In Fig. 4(b), each detected antibiotic has a unique value of $I_{545 \text{ nm}}/I_{618 \text{ nm}}$ according to the luminescence spectra of LOF-S3. For example, the emission intensity ratio of nalidixic acid-LOF is increased from 0.80 (LOF-S3) to 1.54, while $I_{545 \text{ nm}}/I_{618 \text{ nm}}$ of tetracycline-LOF is decreased to 0.61.

The above results illustrated emission intensities of LOF-S3 were responsive to the adsorbed antibiotics by affecting the energy transfer from organic ligand to metal ions. However, the quenching or enhancing influence on the absolute emission intensity of a single ion transition, which is widely detected in the emission spectra of MOF sensors, is inconspicuous for distinguishing some antibiotics. For instance, the absolute emission intensity of Tb^{3+} of chloramphenicol-LOFs was close to that of lincomycin-LOFs, while the absolute emission intensities of Eu^{3+} of nalidixic acid-LOFs and tetracycline-LOFs were almost the same. These results suggest the antibiotic molecules adjusted the energy transfer efficiency from “antenna” ligand (BTC) to metal ions (Eu^{3+} and Tb^{3+}) as well as modulated the energy allocation between different lanthanide ions. To date, most of the fluorescent detection methods of antibiotics rely on a single luminescent site, which is quantified by the change of fluorescence intensity (Table S2). As a result, most of the sensors are only capable of selectively detecting one or two antibiotics. Compared to those single-metal LOF sensors, the self-referring strategy of LOF-S3 amplified the relative emission ratios, which can further enlarge the signals in probing different antibiotics and make decoding antibiotics be easily realized. In addition, this self-calibrating method based on intensity ratios is more reliable as the errors of powder emission intensity are usually unavoidable and uncontrollable (Zhan et al., 2014).

Meanwhile, since the guest included mixed-LOF is a very complex system, minor structural differences are capable of modulating the pathway and allocation of energy transmission. To further investigate the effect of different functional groups, the antibiotics with similar structures but different functional groups were used (Table S3). Remarkably, as shown in Figs. 5(a) and 5(b), the sulfonamide antibiotics (sulfadiazine, sulfamerazine, sulfaclozine, sulfameter, and sulfachinoxalin), which have similar sulfa-structures, are unambiguously recognized by

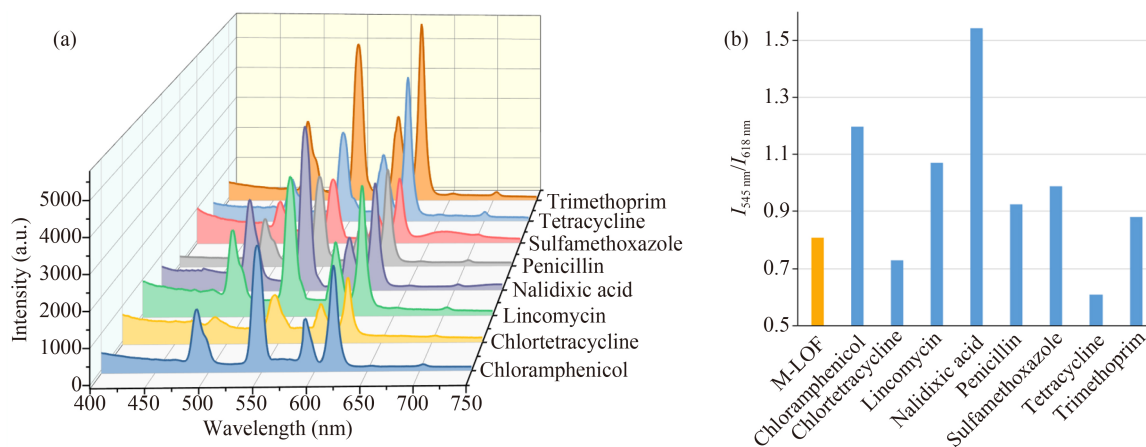


Fig. 4 (a) Emission spectra and (b) intensity ratios ($I_{545 \text{ nm}}/I_{618 \text{ nm}}$) of LOF-S3 after the adsorption of antibiotics ($\lambda_{\text{ex}} = 286 \text{ nm}$).

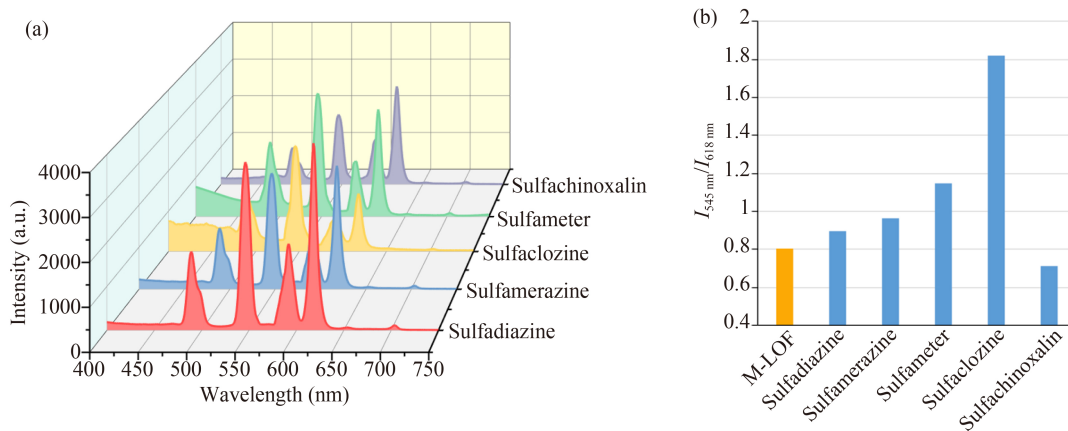


Fig. 5 (a) Emission spectra and (b) emission intensity ratios ($I_{545 \text{ nm}}/I_{618 \text{ nm}}$) of LOF-S3 after the adsorption of sulfonamide antibiotics ($\lambda_{\text{ex}} = 286 \text{ nm}$).

LOF-S3. Compared with sulfadiazine, sulfamerazine and sulfameter have another functional group $-\text{CH}_3$ and $-\text{OCH}_3$, respectively. Both functional groups quench the emission intensity of Eu^{3+} and the quenching effect $-\text{OCH}_3 > -\text{CH}_3$. Moreover, the emission intensity ratio of sulfaclozine-LOF changes to 1.85, while the emission intensity ratio of sulfachinoxalin-LOF is 0.71. The results indicated that $-\text{Cl}$ could enhance the emission intensity of terbium, which was confirmed in the detection of chlorotetracycline (compared to tetracycline). On the contrary, in sulfachinoxalin, an additional benzene ring significantly enhanced the emission intensity of europium.

Since each Ln ion shows more than one characteristic emission peak, with the pristine LOF as the origin, the variation of different peak intensity ratios can set up a unique coordinate for each antibiotic on the map. Therefore, a dual-readout 2D decoded map was established to distinguish 13 antibiotics more visually (Fig. 6). The information on every antibiotic could be achieved from the value of $I_{545 \text{ nm}}/I_{618 \text{ nm}}$ and $I_{592 \text{ nm}}/I_{488 \text{ nm}}$ in LOF-S3 spectra. An antibiotic occupies a unique 2D readout (x-axis: $(R_1 - R_{L1})/R_{L1} \times 100\%$, y-axis: $(R_2 - R_{L2})/R_{L2} \times 100\%$, where $R_1 = I_{545 \text{ nm}}/I_{618 \text{ nm}}$ of the antibiotic, $R_2 = I_{592 \text{ nm}}/I_{488 \text{ nm}}$ of the antibiotic, $R_{L1} = I_{545 \text{ nm}}/I_{618 \text{ nm}}$ of pure LOF-S3, $R_{L2} = I_{592 \text{ nm}}/I_{488 \text{ nm}}$ of pure LOF-S3) in the decoded map. The results reveal that various antibiotics of a certain concentration can be located in one 2D decoded map based on the mixed-LOF sensor. In the first quadrant, the luminescence of Tb is enhanced, and the color of the sensor shifts to green; in the third quadrant, the luminescence of Eu becomes stronger, and the color of the sensor shifts to red. For most antibiotics, R_1 and R_2 change simultaneously, but the deviation of R_1 and R_2 has also been observed ($R_1 \neq R_2$), indicating that the transitions within each lanthanide ion were also affected. As relative intensity (R) was used in this map, no additional intensity calibration was required for LOF-S3, making it a self-calibrating sensor.

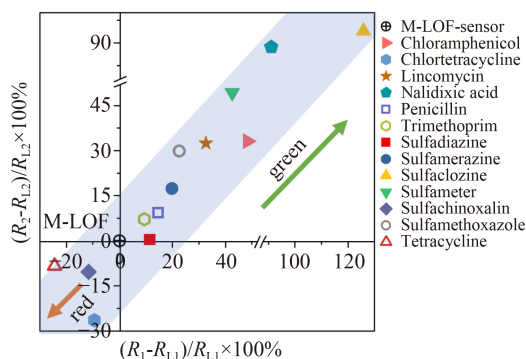


Fig. 6 Decoded map for different antibiotics of LOF-S3 sensor ($\lambda_{\text{ex}} = 286 \text{ nm}$, $R_1 = I_{545 \text{ nm}}/I_{618 \text{ nm}}$ of the antibiotic, $R_2 = I_{592 \text{ nm}}/I_{488 \text{ nm}}$ of the antibiotic, $R_{L1} = I_{545 \text{ nm}}/I_{618 \text{ nm}}$ of LOF-S3, $R_{L2} = I_{592 \text{ nm}}/I_{488 \text{ nm}}$ of LOF-S3).

Scheme S1 shows the possible mechanism of mixed-LOF for sensing antibiotics. In general, the BTC's electrons absorb external energy and are excited to the singlet state (S_1) or second singlet state (S_2). The S_2 state can deactivate to S_1 state through non-radiation deactivation (NRD). Then the S_1 state will be transferred to its triplet state (T_1) through inter-system crossing (ISC). Meanwhile, the energy is transmitted to Tb^{3+} and/or Eu^{3+} via energy transfer which results in the electrons of Tb^{3+} and/or Eu^{3+} being excited to high energy level (5D_4 or 5D_0). Finally, lanthanide ions are deactivated to the ground state via luminescence. However, when the LOF sensor reacts with antibiotics, the antibiotic molecules can cause different interactions or competing with the organic linker, affecting the interior energy transfer in LOF-S3. Thus, the energy transfer efficiency, the energy allocation, and the transitions of Ln ions are adjusted, which enhances or quenches the emission intensity of lanthanide ions in the luminescence spectra of LOF-S3. Assuming the analogous concentration dependence of compound, the decoded map for different concentration

(200 $\mu\text{mol/L}$) is shown in Fig. S6. The 2D readouts for antibiotics in the decoded map are almost double those of the Fig. 6, suggesting that the intensity ratio and antibiotic concentration might exhibit a linear correlation within a certain range. Thus, the intensity ratios of each antibiotic at different concentrations were recorded and the limit of detection (LOD) was calculated according to S2. Limit of detection. The results are shown in Table S3. Among these antibiotics, sulfaclozine and nalidixic acid possess relatively lower detection limits of 0.25 and 0.29 $\mu\text{mol/L}$, respectively. In general, at a certain concentration, the more obvious the change of the mixed-LOF intensity ratio, the lower the detection limit.

Furthermore, the quantitative relationship between the concentration of antibiotics and the intensity ratio of LOF-S3 was investigated. Nalidixic acid (NA) was selected as the target compound. The plot reveals that in the range of 1–200 $\mu\text{mol/L}$, a linear relationship is retained between the concentration of nalidixic acid and the intensity ratio with a slope of about 0.00863 (Fig. 7(a)), indicating that LOF-S3 is a self-referencing fluorescent indicator. To further understand the sensing mechanism of LOF-S3, photoluminescence decay dynamics were measured. According to the emission spectra and decay

curves of LOF-S3 before and after the detection of NA, the emission intensities of both Tb^{3+} and Eu^{3+} decrease as the NA added (Figs. 7(b) and S7), while the average decay lifetimes of Tb^{3+} and Eu^{3+} increase (Table S4). Therefore, the detection of nalidixic acid is may involve a complex modulation process.

The response mechanism of this ratiometric sensor can be explained by the modulation of the energy transfer process in the mixed-LOFs. In original LOF-S3, the energy transfer from BTC to Tb^{3+} and Eu^{3+} leads to the orange emission. After NA is added, since NA mainly exists in the form of anion in water with a carboxyl group, NA molecules can chelate with lanthanide ions and replace the coordinated water. Additionally, the strong absorption of NA at about 280 nm overlaps with the excitation spectrum of mixed-LOF (Kumar et al., 2008). Therefore, in solid samples, UV light is absorbed both by the adsorbed NA and BTC linkers. The competition between NA and BTC may reduce the “antenna effect” of BTC, but at the same time NA can also replace part of the BTC linkers, transferring energy to lanthanide ions. Changes in the energy transfer pathway affect the emission intensity and the decay lifetime (Fig. 7(c)). However, the intensity changes of the two lanthanide

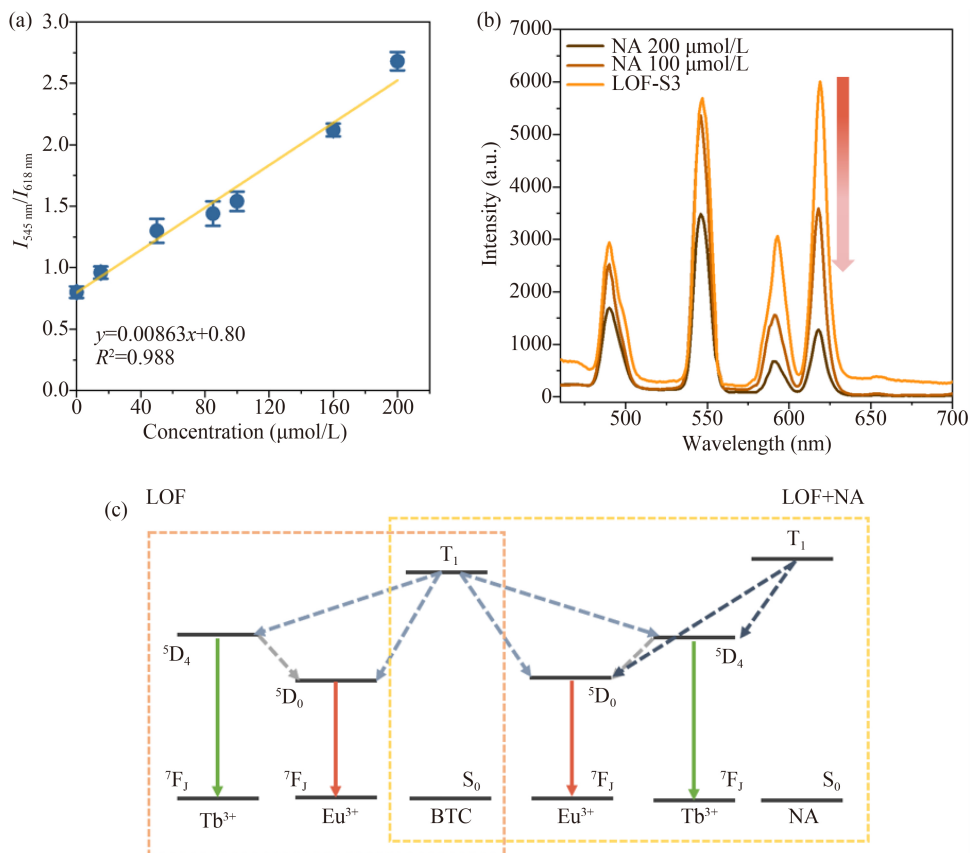


Fig. 7 (a) Intensity ratios ($I_{545\text{ nm}}/I_{618\text{ nm}}$) of LOF-S3 in the presence of different concentrations of nalidixic acid ($\lambda_{\text{ex}} = 286\text{ nm}$); (b) Emission spectra of LOF-S3 before and after the detection of nalidixic acid; (c) possible mechanism of LOF-S3 sensing for nalidixic acid.

metal elements are not synchronized, and the intensity reduction of Eu^{3+} is much more than that of Tb^{3+} , which may be explained by the following reasons: (1) The binding energy calculated by Material Studio 7.0 shows that the binding energy of Tb-BTC and NA (ca. -751 kcal/mol) is higher than that of Eu-BTC and NA (ca. -705 kcal/mol), indicating that NA is more inclined to bind to Tb-BTC in mixed-LOF system. NA can also coordinate with the Eu^{3+} ions, but there are far more Tb atoms than Eu in LOF-S3, which further reduces the coordination probability of Eu^{3+} . (2) According to the previous research, the triplet energy level of NA is about 27016 cm^{-1} (Monti et al., 2008), which is more suitable for sensitizing Tb^{3+} ions (ca. 20500 cm^{-1}) (Zhang et al., 2016a). (3) The phonon vibrations in the EuTb-BTC lattice can be affected by the coordination of NA^- and Tb^{3+} . Because the energy transfer from Tb^{3+} to Eu^{3+} is mainly controlled by the phonon-assisted Förster transfer mechanism, the Tb-to-Eu energy transfer is further affected (Rao et al., 2013; Zhou et al., 2015). These reasons lead to a significant drop in the red emission of Eu and an increase in the value of $I_{545\text{ nm}}/I_{618\text{ nm}}$.

For a luminescent sensor, reusability is essential for real-world applications. After detection, the re-collected samples were washed by organic solvent (methanol, DMF) and dried for 12 h. In the recycling experiment, the sensing of nalidixic acid by the solid sample of LOF-S3 was still efficient after five cycles. As shown in Fig. 8, the emission intensity ratio $I_{545\text{ nm}}/I_{618\text{ nm}}$ hardly changes. The results demonstrated the reversible properties of LOF-S3, which can be reused and recycled for the subsequent detection.

It is not easy to separate powder samples from the liquid medium. Thus, to meet practical requirements, we explored the immobilization of LOF-S3 on solid substrates. Post-synthetic modification is an effective strategy. The mixed-LOF was integrated with polymers to

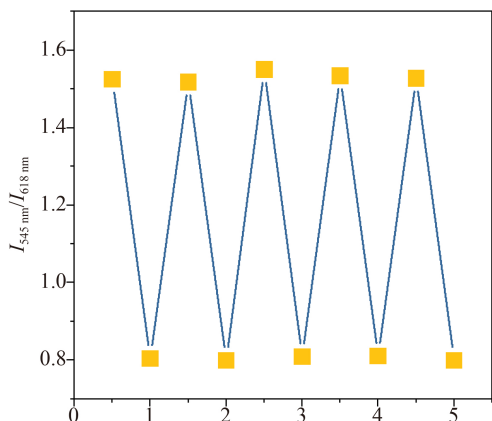


Fig. 8 Recycling probing of nalidixic acid by LOF-S3: the integrated emission intensity ratios ($I_{545\text{ nm}}/I_{618\text{ nm}}$) after adsorption and desorption of nalidixic acid (200 mL 100 $\mu\text{mol/L}$ nalidixic acid solution, 5 mg Ln-BTC, $\lambda_{\text{ex}} = 286\text{ nm}$).

form a fibrous composite via electrospinning (Fig. 9(a)). The fluorescent characteristics were further explored. In Fig. 9(b), the sharp peaks at 592, 488, 545, and 618 nm and the emission intensity ratios are consistent with those of the powder sample. The amount of LOF integrated with polymers was verified to investigate its effect on the luminescence of LOF-S3 fibers. The intensity ratios ($I_{545\text{ nm}}/I_{618\text{ nm}}$) of LOF-S3 fibers with different amounts of LOFs during synthesis were recorded. In Fig. S8, the values of $I_{545\text{ nm}}/I_{618\text{ nm}}$ in LOF-S3 fibers remain stable with the increasing amount of LOF-S3. However, after adding nalidixic acid, the change of intensity ratio ($I_{545\text{ nm}}/I_{618\text{ nm}}$) decreases with the increasing amount of LOF-S3, which is due to the decrease in the number of nalidixic acid molecules that could be adsorbed by LOF-S3 per unit mass. It should also be noted that low LOF loading results in weaker fluorescence emission. Therefore, the amount of LOF integrated with polymers was chosen to be 0.1 g in this work.

To investigate the stability and durability of LOF-S3 fibers, the material was immersed in aqueous solutions of varying pH and ionic strength. As shown in Figs. S9a and S9b, the emission intensity ratios of LOF-S3 fibers ($I_{545\text{ nm}}/I_{618\text{ nm}}$) keep stable. In addition, the XRD patterns of LOF-S3 fibers is basically unchanged after storage in water for several days (Fig. S9c), indicating that the mixed-LOF fibrous composite can maintain the stability in aqueous solution. Additionally, the response signals ($I_{545\text{ nm}}/I_{618\text{ nm}}$) remain stable in simulated natural samples such as simulated river water and PBS buffer (Fig. S9d). NA was used as the representative antibiotic to estimate the performance of LOF-S3 fibers. With increasing NA concentrations, the LOF-S3 fibers exhibits a color change from orange to yellow-green under fluorescence microscope (Fig. 9c). The color information (RGB values) can be obtained by color extraction with a smartphone for estimating NA concentrations. Therefore, as illustrated in Fig. 9d, the LOF-S3 fibers can be connected to the device to perform as a portable sensor.

4 Conclusions

In summary, this study synthesized luminescent mixed-LOFs and used the most suitable one as a self-calibrating sensor for visual decoding and quantitative detection of antibiotics. In this system, highly efficient resonance energy transferred from the organic linker to metal ions was achieved because the emission band of BTC matched well with the excitation band of $\text{Eu}^{3+}/\text{Tb}^{3+}$. The photoluminescence decay curves indicated the energy transfer from Tb^{3+} to Eu^{3+} occurred. The energy transfer efficiency from BTC to Ln ions, the energy allocation between different Ln ions, and the interior transitions of Ln ions could be influenced by the analytes. Therefore, by converting the influence of guest molecules into the

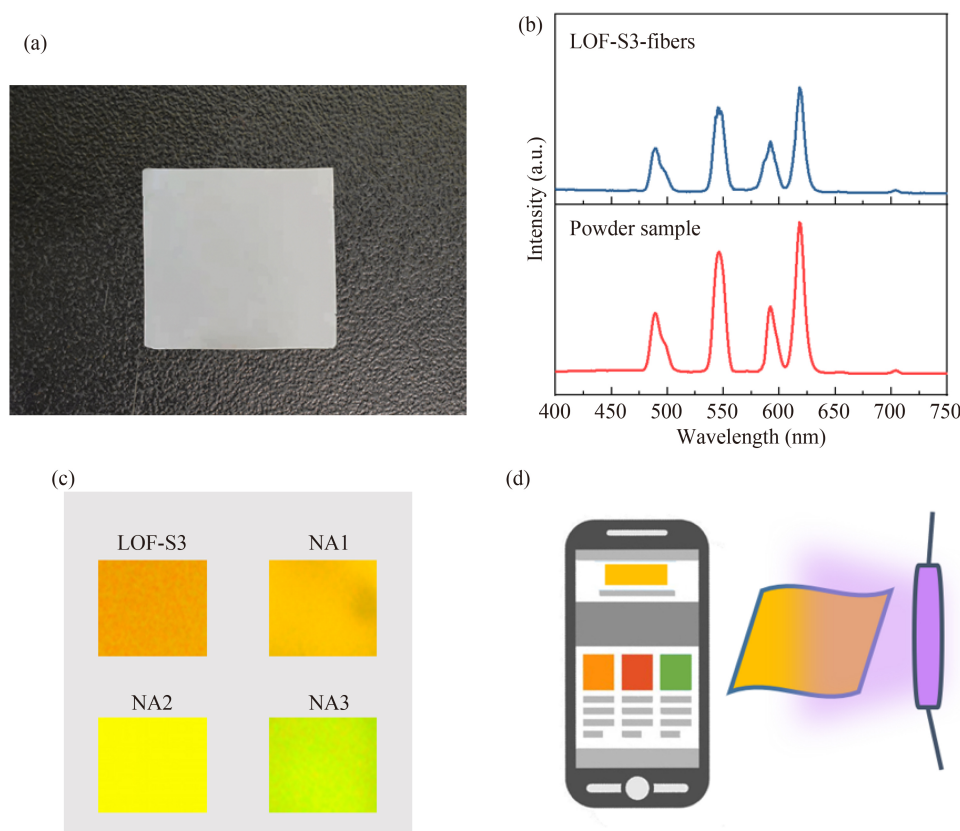


Fig. 9 (a) Images and (b) luminescence spectra of LOF-S3 fibers; (c) the optical photographs for mixed-LOF fibers under fluorescence microscope before and after the detection of nalidixic acid (NA 1: 50 $\mu\text{mol/L}$, NA 2: 100 $\mu\text{mol/L}$, NA 3: 200 $\mu\text{mol/L}$); (d) Schematic diagram for the detection of antibiotics using a smartphone.

variation of emission intensity ratios, different antibiotics were simply differentiated. A 2D decoded map for antibiotics was established where every antibiotic was represented by a unique dual-readout. The linear relationship between the concentration of NA and the emission intensity ratio indicated the quantitative determination of antibiotics was feasible. The competition in the absorption of UV light between NA and BTC affected the energy transfer, resulting in a significant drop in the red emission of Eu and an increase in the value of $I_{545\text{ nm}}/I_{618\text{ nm}}$. To prepare a portable sensor for real-world applications, LOF-S3 was integrated with polymer fibers. The stability and durability of LOF-S3 fibers were also confirmed. The proposed LOF-S3 fibers show the potential in recognition and monitoring antibiotics through a detection platform. Our findings on the luminescent responses of LOF-S3 toward different antibiotics provide valuable insights into the design and development of multifunctional LOF sensors for beneficial applications.

Acknowledgements This study was supported by the 2020 Young Teacher Education Project of Fujian Provincial Department of Education (No. JAT200008) and the 2017 Major Science and Technology Program for Water Pollution Control and Treatment (No. 2017ZX07202).

Electronic Supplementary Material Supplementary material is available

in the online version of this article at <https://doi.org/10.1007/s11783-022-1589-5> and is accessible for authorized users.

References

- Brites C D, Lima P P, Silva N J, Millán A, Amaral V S, Palacio F, Carlos L D (2010). A luminescent molecular thermometer for long-term absolute temperature measurements at the nanoscale. *Advanced Materials*, 22(40): 4499–4504
- Chatterton N, Bretonnière Y, Pécaut J, Mazzanti M (2005). An efficient design for the rigid assembly of four bidentate chromophores in water-stable highly luminescent lanthanide complexes. *Angewandte Chemie (International ed. in English)*, 44(46): 7767–7770
- Cheng D, Ngo H H, Guo W, Chang S W, Nguyen D D, Liu Y, Wei Q, Wei D (2020). A critical review on antibiotics and hormones in swine wastewater: Water pollution problems and control approaches. *Journal of Hazardous Materials*, 387: 121682
- Chiesa L, Panseri S, Pasquale E, Malandra R, Pavlovic R, Arioli F (2018). Validated multiclass targeted determination of antibiotics in fish with high performance liquid chromatography-benchtop quadrupole orbitrap hybrid mass spectrometry. *Food Chemistry*, 258: 222–230
- Dolgoplova E A, Rice A M, Martin C R, Shustova N B (2018). Photochemistry and photophysics of MOFs: Steps towards MOF-based sensing enhancements. *Chemical Society Reviews*, 47(13):

- 4710–4728
- Eliseeva S V, Bünzli J C G (2010). Lanthanide luminescence for functional materials and bio-sciences. *Chemical Society Reviews*, 39(1): 189–227
- Gao Y, Yu G, Liu K, Wang B (2018). Luminescent mixed-crystal Ln-MOF thin film for the recognition and detection of pharmaceuticals. *Sensors and Actuators. B, Chemical*, 257: 931–935 doi:10.1016/j.snb.2017.10.180
- Hernández M, Borrull F, Calull M (2003). Analysis of antibiotics in biological samples by capillary electrophoresis. *Trends in Analytical Chemistry*, 22(7): 416–427
- Horcajada P, Serre C, Maurin G, Ramsahye N A, Balas F, Vallet-Regí M, Sebba M, Taulelle F, Férey G (2008). Flexible porous metal-organic frameworks for a controlled drug delivery. *Journal of the American Chemical Society*, 130(21): 6774–6780
- Hou S L, Dong J, Tang M H, Jiang X L, Jiao Z H, Zhao B (2019). Triple-interpenetrated lanthanide-organic framework as dual wave bands self-calibrated pH luminescent probe. *Analytical Chemistry*, 91(8): 5455–5460
- Hu Y, Jin L, Zhao Y, Jiang L, Yao S, Zhou W, Lin K, Cui C (2021). Annual trends and health risks of antibiotics and antibiotic resistance genes in a drinking water source in East China. *Science of the Total Environment*, 791: 148152
- Karmakar S, Ghosh A, Prasad K, Rahimi F A, Rambabu D, Haldar R, Maji T K (2021). Multicolour lanthanide(III) porous 1D coordination polymers: Tunable wide spectrum emission and efficient Cu^{II} sensing. *Dalton Trans*, 50(37): 13002–13011
- Kökçam-Demir Ü, Goldman A, Esrafilı L, Gharib M, Morsali A, Weingart O, Janiak C (2020). Coordinatively unsaturated metal sites (open metal sites) in metal-organic frameworks: Design and applications. *Chemical Society Reviews*, 49(9): 2751–2798
- Kovalakova P, Cizmas L, McDonald T J, Marsalek B, Feng M, Sharma V K (2020). Occurrence and toxicity of antibiotics in the aquatic environment: A review. *Chemosphere*, 251: 126351
- Kumar A, Kumar Malik A, Kumar Tewary D, Singh B (2008). Gradient HPLC of antibiotics in urine, ground water, chicken muscle, hospital wastewater, and pharmaceutical samples using C-18 and RP-amide columns. *Journal of Separation Science*, 31(2): 294–300
- Monti S, Manet I, Manoli F, Capobianco M L, Marconi G (2008). Gaining an insight into the photoreactivity of a drug in a protein environment: A case study on nalidixic acid and serum albumin. *Journal of Physical Chemistry. B*, 112(18): 5742–5754
- Moore E G, Samuel A P, Raymond K N (2009). From antenna to assay: lessons learned in lanthanide luminescence. *Accounts of Chemical Research*, 42(4): 542–552
- Peterson G W, Lee D T, Barton H F, Epps T H III, Parsons G N (2021). Fibre-based composites from the integration of metal-organic frameworks and polymers. *Nature Reviews. Materials*, 6(7): 605–621
- Rao X, Song T, Gao J, Cui Y, Yang Y, Wu C, Chen B, Qian G (2013). A highly sensitive mixed lanthanide metal-organic framework self-calibrated luminescent thermometer. *Journal of the American Chemical Society*, 135(41): 15559–15564
- Roth T, Weber L, Niestroj M, Cipa F, Löscher A, Mihai S, Parsch H (2021). Simultaneous determination of six antibiotics in human serum by high-performance liquid chromatography with UV detection. *Biomed Chromatogr*, 35(3): e5010
- Shu Y, Ye Q, Dai T, Guan J, Ji Z, Xu Q, Hu X (2022). Incorporation of perovskite nanocrystals into lanthanide metal-organic frameworks with enhanced stability for ratiometric and visual sensing of mercury in aqueous solution. *Journal of Hazardous Materials*, 430: 128360
- Wang R, Ji M, Zhai H, Guo Y, Liu Y (2021). Occurrence of antibiotics and antibiotic resistance genes in WWTP effluent-receiving water bodies and reclaimed wastewater treatment plants. *Science of the Total Environment*, 796: 148919
- Wu S, Min H, Shi W, Cheng P (2020). Multicenter metal-organic framework-based ratiometric fluorescent sensors. *Advanced Materials*, 32(3): 1805871
- Xia T, Wan Y, Li Y, Zhang J (2020). Highly stable lanthanide metal-organic framework as an internal calibrated luminescent sensor for glutamic acid, a neuropathy biomarker. *Inorganic Chemistry*, 59(13): 8809–8817
- Xu L, Zhang H, Xiong P, Zhu Q, Liao C, Jiang G (2021). Occurrence, fate, and risk assessment of typical tetracycline antibiotics in the aquatic environment: A review. *Science of the Total Environment*, 753: 141975
- Yang A F, Hou S L, Shi Y, Yang G L, Qin D B, Zhao B (2019). Stable lanthanide-organic framework as a luminescent probe to detect both histidine and aspartic acid in water. *Inorganic Chemistry*, 58(9): 6356–6362
- Yu H, Liu Q, Li J, Su Z M, Li X, Wang X, Sun J, Zhou C, Hu X (2021). A dual-emitting mixed-lanthanide MOF with high water-stability for ratiometric fluorescence sensing of Fe³⁺ and ascorbic acid. *Journal of Materials Chemistry. C, Materials for Optical and Electronic Devices*, 9(2): 562–568
- Zeng X, Hu J, Zhang M, Wang F, Wu L, Hou X (2020). Visual detection of fluoride anions using mixed lanthanide metal-organic frameworks with a smartphone. *Analytical Chemistry*, 92(2): 2097–2102
- Zhan C, Ou S, Zou C, Zhao M, Wu C D (2014). A luminescent mixed-lanthanide-organic framework sensor for decoding different volatile organic molecules. *Analytical Chemistry*, 86(13): 6648–6653
- Zhang Y, Li B, Ma H, Zhang L, Jiang H, Song H, Zhang L, Luo Y (2016a). A nanoscaled lanthanide metal-organic framework as a colorimetric fluorescence sensor for dipicolinic acid based on modulating energy transfer. *Journal of Materials Chemistry. C, Materials for Optical and Electronic Devices*, 4(30): 7294–7301
- Zhang Y, Li B, Ma H, Zhang L, Zheng Y (2016b). Rapid and facile ratiometric detection of an anthrax biomarker by regulating energy transfer process in bio-metal-organic framework. *Biosensors & Bioelectronics*, 85: 287–293
- Zhou J, Li H, Zhang H, Li H, Shi W, Cheng P (2015). A bimetallic lanthanide metal-organic material as a self-calibrating color-gradient luminescent sensor. *Advanced Materials*, 27(44): 7072–7077